

A Gd@C₈₂ single-molecule electret

Kangkang Zhang[®]¹,¹¹, Cong Wang[®]²,¹¹, Minhao Zhang¹,¹¹, Zhanbin Bai¹,¹¹, Fang-Fang Xie³, Yuan-Zhi Tan[®]³, Yilv Guo⁴, Kuo-Juei Hu¹, Lu Cao¹, Shuai Zhang[®]¹, Xuecou Tu[®]⁵, Danfeng Pan⁵, Lin Kang⁵, Jian Chen⁵, Peiheng Wu⁵, Xuefeng Wang⁵, Jinlan Wang⁴, Junming Liu[®]¹, You Song[®]⁶, Guanghou Wang[®]¹, Fengqi Song[®]¹, Wei Ji[®]², Su-Yuan Xie[®]³, Su-Fei Shi[®]8,9, Mark A. Reed[®]¹® and Baigeng Wang¹

Electrets are dielectric materials that have a quasi-permanent dipole polarization. A single-molecule electret is a long-sought-after nanoscale component because it can lead to miniaturized non-volatile memory storage devices. The signature of a single-molecule electret is the switching between two electric dipole states by an external electric field. The existence of these electrets has remained controversial because of the poor electric dipole stability in single molecules. Here we report the observation of a gate-controlled switching between two electronic states in $Gd@C_{82}$. The encapsulated Gd atom forms a charged centre that sets up two single-electron transport channels. A gate voltage of $\pm 11V$ (corresponding to a coercive field of ~50 mV Å-1) switches the system between the two transport channels with a ferroelectricity-like hysteresis loop. Using density functional theory, we assign the two states to two different permanent electrical dipole orientations generated from the Gd atom being trapped at two different sites inside the C_{82} cage. The two dipole states are separated by a transition energy barrier of 11 meV. The conductance switching is then attributed to the electric-field-driven reorientation of the individual dipole, as the coercive field provides the necessary energy to overcome the transition barrier.

he miniaturization of modern electrical devices has been approaching the single atomic or molecular scale¹, which has ignited research into single-molecule devices (SMDs). Many efforts have been made to fabricate SMDs and design functional devices such as switches²⁻⁶, diodes⁷⁻¹⁰, transistors¹¹⁻¹⁵ and sensors¹⁶⁻¹⁸, which are promising building blocks of future molecular computers19. Among these molecules, fullerenes and their derivatives stand out^{11,20} due to their unique cage-like structures. C₆₀-based SMDs have shown numerous interesting physics and striking properties, such as the Kondo effect²¹, quantum phase transition²², superconductivity²³ and negative differential resistance²⁴. Furthermore, foreign atoms can be introduced into fullerene cages; these electric charge or magnetic centres can strengthen superconductivity²⁵, or, like in the case of a caged N atom, show protection of a quantum information cage with a coherence time of up to 0.23 ms (ref. ²⁶). In addition, cage size has also been shown to have a physical effect. For example, C_{82} has a deformed cage with lower symmetry than C_{60} and RE@C₈₂ species (RE = La, Gd, Tb, Dy, Ho, Er) have been studied as small and stable memory storage units^{27–30}. In particular, Ce@C₈₂ (ref. 31) has even demonstrated hysteresis in transport characteristics attributed to nanomechanical rearrangement. Such efforts lead to interest in molecules with non-superimposable charge centres and structural centres32,33, which may form stabilized electric dipoles in the molecule, exhibiting ferroelectric characteristics without long-range dipole ordering. This would then realize the long-sought single-molecule electret (SME). Here we show the gate-controlled switching between two sets of characteristic single-electron stability diagrams in the electrical transport of a Gd@C $_{82}$ -based SMD. It is fabricated by a feedback-controlled electromigration break junction (FCEBJ) method 11 and can be operated in a hysteresis loop with a coercive gate field of $\sim 50\, \text{mV}$ Å $^{-1}$. Based of density functional theory calculations, we interpret the switching as the electrical-field-driven reorientation of a single molecular dipole, thus providing definitive evidence of a SME switching device.

Single-electron transport in Gd@C₈₂ transistors

As schematically shown in Fig. 1a, the single $Gd@C_{82}$ molecular transistor is prepared by setting a $Gd@C_{82}$ molecule into a pair of Au electrodes that have a nanometre-scale gap, which is fabricated according to the details provided in the Methods section. Figure 1b shows a set of current–voltage (I-V) curves in a typical FCEBJ procedure¹¹, and the device's morphology is shown in the inset. Care is taken during the thermal oxide growth to achieve a satisfactory gating efficiency and local gating field, which are critical in this $Gd@C_{82}$ study with a sizeable density of states near the Fermi level. We etch the previously thick SiO_2 using dilute HF, then regrow a new layer of SiO_2 of about 30 nm by a dry oxidation method, repeated twice.

A back gate of 7–10 V can modulate the *I–V* curve (Fig. 1c). A nonlinear dependence between the current and the voltage can be

National Laboratory of Solid State Microstructures, Collaborative Innovation Center of Advanced Microstructures, and School of Physics, Nanjing University, Nanjing, China. ¹Beijing Key Laboratory of Optoelectronic Functional Materials and Micro-Nano Devices, and Department of Physics, Renmin University of China, Beijing, China. ³State Key Laboratory of Physical Chemistry of Solid Surfaces and Department of Chemistry, College of Chemistry and Chemical Engineering, Xiamen University, Xiamen, China. ⁴School of Physics, Southeast University, Nanjing, China. ⁵School of Electronic Science and Engineering and Collaborative Innovation Center of Advanced Microstructures, Nanjing University, Nanjing, China. ⁵State Key Laboratory of Coordination Chemistry, Collaborative Innovation Center of Advanced Microstructures, School of Chemistry and Chemical Engineering, Nanjing University, Nanjing, China. ⁵Atomic Manufacture Institute, Nanjing, China. ®Department of Chemical and Biological Engineering, Rensselaer Polytechnic Institute, Troy, NY, USA. ®Department of Electrical, Computer and Systems Engineering, Rensselaer Polytechnic Institute, Troy, NY, USA. ®Departments of Applied Physics and Electrical Engineering, Yale University, New Haven, CT, USA. ™These authors contributed equally: Kangkang Zhang, Cong Wang, Minhao Zhang, Zhanbin Bai. ™e-mail: songfengqi@nju.edu.cn; wji@ruc.edu.cn; syxie@xmu.edu.cn; shis2@rpi.edu; mark.reed@yale.edu

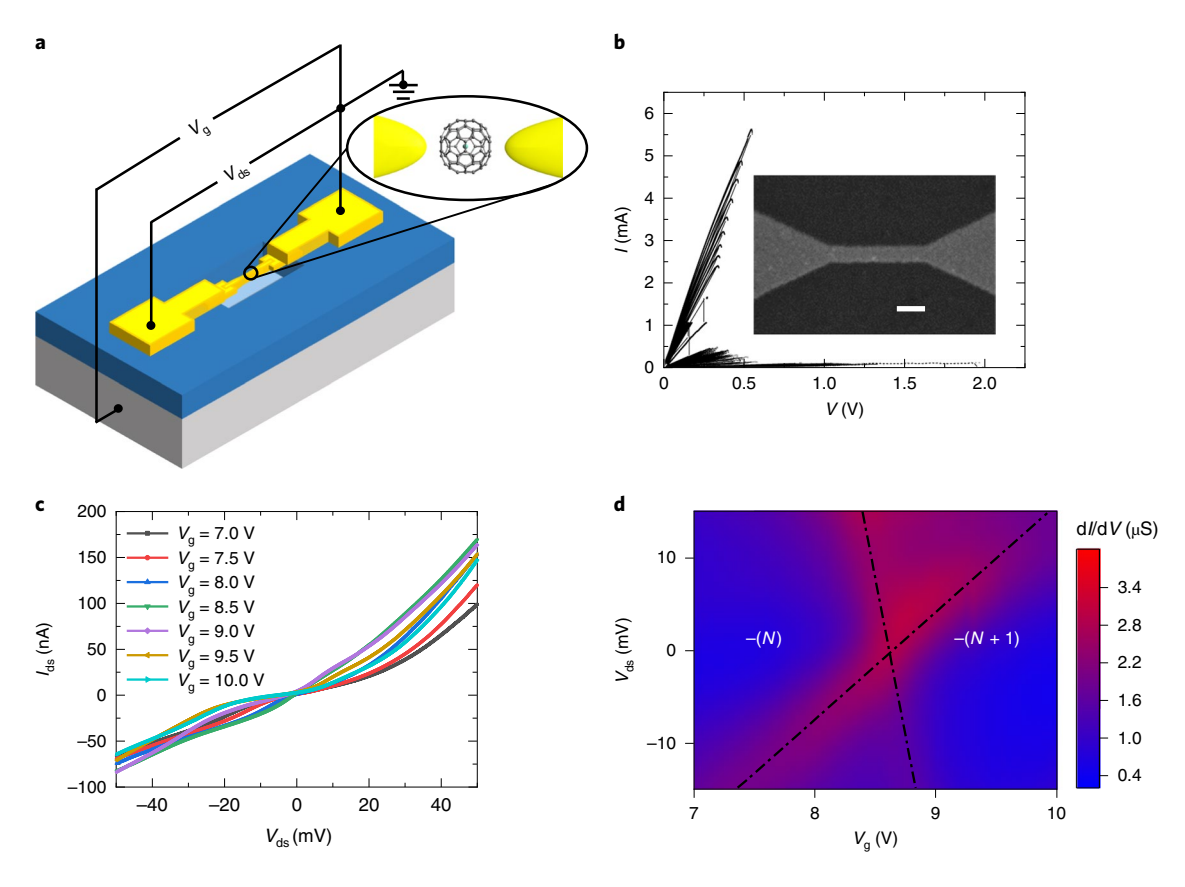


Fig. 1 | Single-electron transport of the $Gd@C_{82}$ SMD. a, The SMD configuration. A single $Gd@C_{82}$ molecule bridges a nanogap in a pair of bow-tie gold electrodes on top of a 30-nm-thick silicon dioxide layer. b, A typical feedback-controlled electromigration process. The inset is a scanning electron microscope image of the Au nanoelectrode before it was broken. Scale bar, 100 nm. c, Representative I(V) curves for different gate voltages V_g after the electromigration. d, Differential conductance dI/dV plotted against the bias voltage V_{ds} and the gate voltage V_g . The blue regions are the Coulomb blockade areas, and the red lines show peaks in the differential conductance. This shows the operation from N to N+1 electrons.

seen, and there is a current blockade area at low voltage. The gate voltage can decrease or increase the blockade voltage range, indicating change in the electrochemical potential. A plot of the differential conductance dI/dV as a function of the bias voltage V_{ds} and the gate voltage $V_{\rm g}$ is shown in Fig. 1d. The differential conductance is derived by numerical differentiation of the current with respect to the bias voltage. The blue regions are the Coulomb blockade regions, and the red regions show differential conductance peaks. For clarity, two black dashed lines are shown in Fig. 1d to indicate the SMD Coulomb edges. Changing the gate voltage will tune the chemical potential of the molecule. When the electrochemical potential is aligned with the Fermi energy of the source and drain electrodes, the conductance gap will decrease to zero and reach a degeneracy point (where the two black dashed lines cross), indicating the successful preparation of a single-electron transistor with a Gd@C₈₂ SMD. With a larger gate voltage scan, multiple peaks are observed (Supplementary Fig. 1), indicating that our SMD could access a series of redox states and degeneracy points. Such multiple degeneracy points have been previously related to the molecular energy levels14.

Gate-controlled switching between two electronic states, and its hysteresis loop

An interesting switching between two molecular states is observed. We carefully measure the current as a function of the gate voltage when the source–drain bias is fixed at 2 mV (Fig. 2a). The gate voltage is swept backward and forward over a large range. In contrast to the literature^{11,14}, the source–drain current shows two sets of

Coulomb oscillation patterns. The red and green curves are similar, defined as **State 1**, and the blue curve is defined as **State 2**. The two sets of Coulomb oscillation patterns can be reversibly switched, in contrast to the previous result in $Ce@C_{82}$ (ref. 31), when after application of a large bias voltage, the Coulomb stability diagram is irreversibly changed. Furthermore, the oscillation peaks can be related to the molecular orbitals (as shown later); hence, we speculate that the onset of two sets of oscillation peaks means that $Gd@C_{82}$ may have two metastable states. Our observation suggests that the structure of the molecule can be controlled and switched by the external electric field.

Systematic two-dimensional plots of the differential conductance are measured over a large range of gate voltages, that is, -13to 15 V. The detailed Coulomb stability diagrams of the two states are shown in Fig. 2d,e, which shows a distinct difference. First, the Coulomb degeneracy points are different, corresponding to the Coulomb oscillations at different gate voltages. Second, the slopes of the Coulomb edges, that is, the white line in the plots (black dashed lines are shown in Fig. 2d,e for clarity), are also different. We investigate these differences between the two states quantitatively by using a capacitance model to calculate the SMD's detail parameters34. In Fig. 2d, the ratio of the gate, source and drain conductances $(C_g/C_s/C_d)$ is 1:15.05:133.23, and the gate efficiency factor α is 0.0067 (where $e\alpha V_{g}$ is the change in the electrochemical potential caused by the gate electrode and e is the electron charge). In Fig. 2e, the $C_a/C_s/C_d$ ratio for the three capacitors is 1:15.34:86.97 and the gate efficiency factor α changes to 0.0097. The drastic difference in both gate efficiency and gate capacitances confirms that the SMD

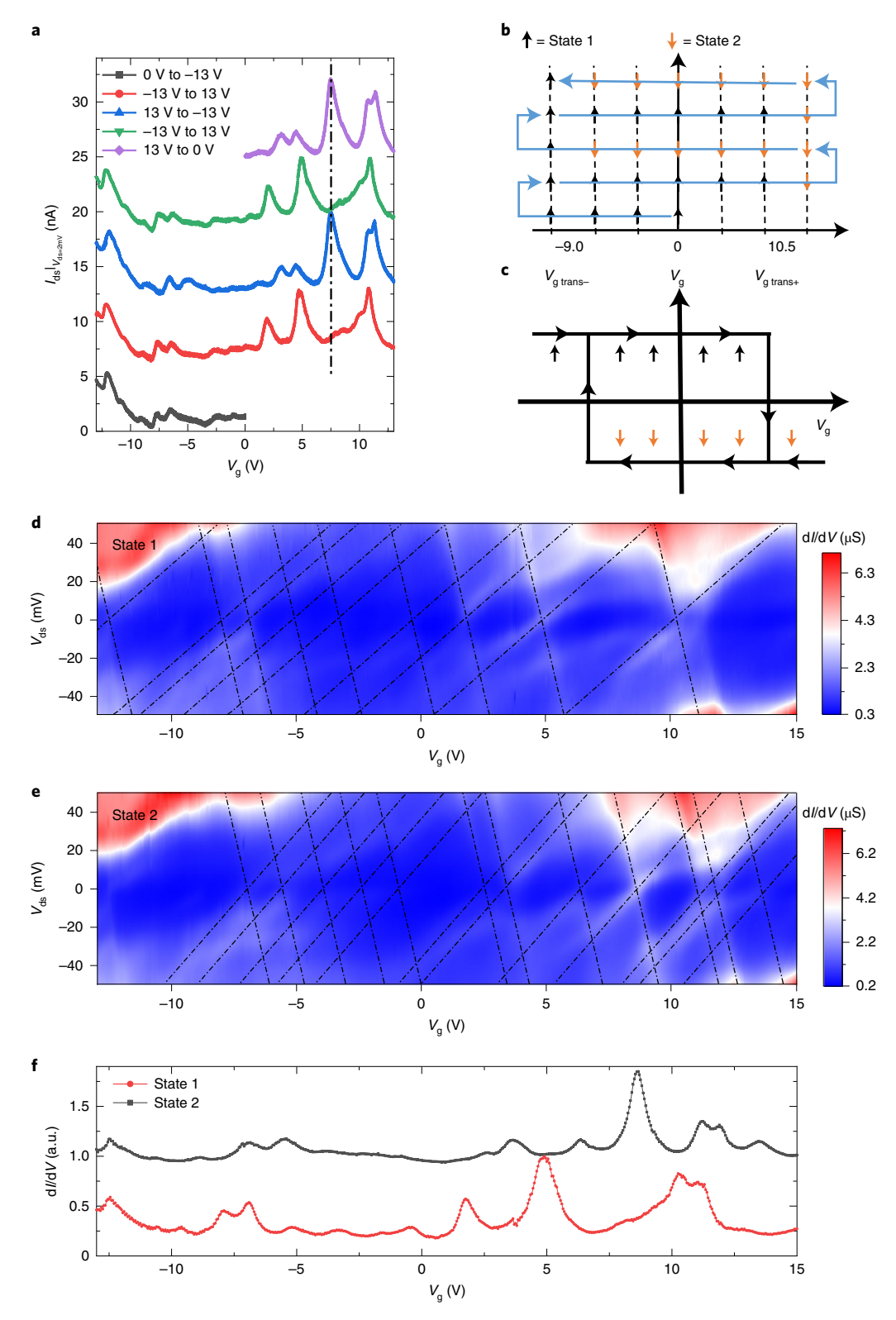


Fig. 2 | Gate-controlled switching between the two molecular states showing a ferroelectricity-like hysteresis loop. **a**, The source-drain current is plotted as a function of the gate voltage with the source-drain bias fixed at 2 mV when the gate voltage was swept backward and forward. The black dashed line marks several resistance points, indicating that two states are accessed. State 1: the red and green curves, with low current while crossing the dashed line. State 2: the other curves, such as the blue curve, with high current while crossing the dashed line. An offset is added to each line for clarity. **b,c**, Schematic of the switching process (**b**). A repeatedly cycled gate voltage switches the SMD between States 1 and 2, whose conductance diagrams are detailed in **d** and **e**, respectively. The arrowed blue line indicates the sequence that the gate voltage is applied. The molecule cannot switch between states unless a large enough gate voltage $V_{g \, trans-}$ / $V_{g \, trans-}$ is applied to the SMD. This indicates the onset of a coercive gate field and leads to a ferroelectricity-like hysteresis loop as shown in **c. d,e**, Colour plot of the differential conductance dI/dV plotted against the bias voltage $V_{d \, s}$ and gate voltage $V_{g \, v}$ over a large voltage range for the device. The voltage increases from $-13 \, V$ to $15 \, V$ in **d**, and does the reverse in **e. f**, A cut line plot of the stability diagram when the bias is $0 \, V$. The red and grey lines are extracted from **d** and **e**, respectively. Arbitrary units and an offset are employed for clarity. All the measurements were performed at a temperature $T = 1.6 \, K$.

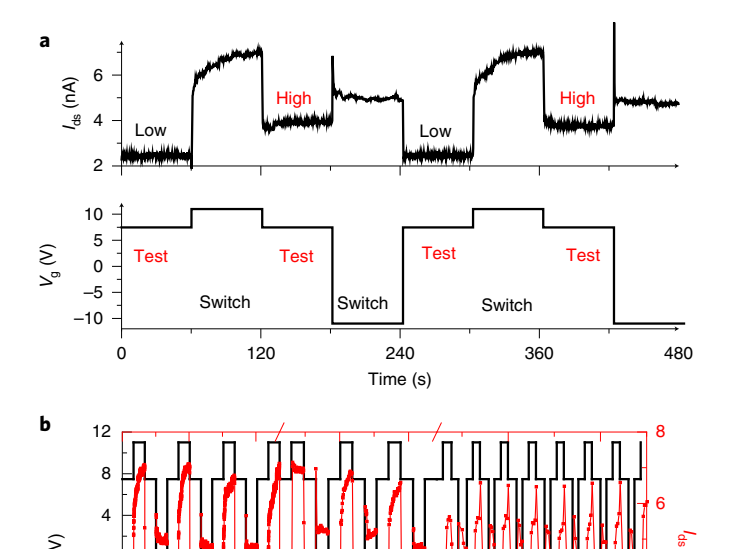


Fig. 3 | Simulating a two-resistance-state operation based on the SMD switching. a, The bottom figure is the gate voltage plotted against time. The switch gate voltage is ± 11 V and the test gate voltage is 7.472 V, using a time step of 60 s. The top figure is the current plotted against the same time as used in the bottom figure, with the bias voltage at 2 mV. The 'test' current switches between the two parts marked 'low' and 'high'. **b**, The switch between two molecular states can be achieved using time steps of 60, 10 and 1s. The black and red lines are the gate voltage and bias current,

900

960

Time (s)

1,000

undergoes a significant change of its electronic states. The difference between these two stability diagrams has its origin in the order in which the gate voltage is applied. Starting from the state Fig. 2d (State 1), the gate voltage is first decreased to $-13\,\rm V$, and then increased to $15\,\rm V$, leading to Fig. 2e (State 2). To emphasize the differences between the two states, two cut lines of Fig. 2d,e (red and grey curves, respectively) are shown in Fig. 2f when the bias voltage is zero. Two subsection plots shown in Supplementary Fig. 2 illustrate the differences between these two stability diagrams. These two sets of stability diagrams are highly repeatable, reproducible and stable for more than one month, indicating that the gate voltage changes the internal structure of the molecule. From the two Coulomb stability diagrams, we can gain further information about these two metastable states of $\rm Gd@C_{82}$ with the aid of theory calculations, as shown below.

Repeatable switching between the two states results in a ferroelectricity-like hysteresis loop with a coercive gate field of around $50\,\text{mV}\,\text{Å}^{-1}$. Analysing the data shown in Fig. 2a, we summarize the switching of the SMD (Fig. 2b), where the thin blue-arrowed line indicates the gate application sequence. We label the diagram of Fig. 2d as the black arrow (State 1) and the diagram of Fig. 2e as the orange arrow (State 2). The starting state is initially set to State 1 when the gate voltage is 0 V. The device maintains State 1 even if we decrease the gate voltage to $-10\,\text{V}$. We then change the gate voltage direction. When the gate voltage is increased positively to over $10.5\,\text{V}$, the device was found to switch to State 2. The state can be set back to State 1 when a large enough negative gate voltage is applied. Such switching or reversal can be reliably reproduced,

as seen in Fig. 2b, which can be understood by the state switching of the molecule driven by the out-of-plane electric field provided by the back-gate voltage. Figure 2b,c essentially depicts a hysteresis loop in typical ferroelectricity operations at the single-molecular level, essentially the evidence of a SME. Another SMD also displays similar results with reversible switching character (Supplementary Fig. 3), although the Coulomb degeneracy points are not exactly the same on different devices, since some small differences in contact morphology can lead to different quantized orbits. We also carried out measurements of the temperature and frequency dependence of the dielectric properties of bulk materials (Supplementary Figs. 4 and 5); we believe the low-temperature relaxation process originates from the reversal of the dipole.

The reliable switching of the two states leads to a series of programmable operations. In fact, any gate voltage point in Fig. 2a can be employed to simulate a two-resistance-state operation and SMD storage, as long as each point has a different current. We select one point in Fig. 2a as an example. In one point of the state, the current is only 2 nA because the SMD was in the blockade state, while in another molecular state the current is 8 nA when the blockade is removed. This operation is shown in Fig. 3a. The switch gate voltage is ±11 V and the test gate voltage is 7.472 V to read the molecular state (the bottom panel of Fig. 3a). The corresponding current as a function of time is shown in the top panel of Fig. 3a, with a bias voltage of 2 mV. The 'test' current takes on two values, marked 'low' and 'high' at the top of Fig. 3a. Different currents (~62% difference) indicate different molecular states, which can be used in a typical two-state electret storage device. The time step could be changed to 10 or 1s (Fig. 3b, in which the red line is the bias current). The figure shows two obviously different currents at the test gate voltage no matter what time step is used, and this observation can be repeated more than 20 times. This confirms that the single Gd@C₈₂ molecular device has two metastable states and can be reliably set and reset by a gate voltage, which we relate to a controlled switching of SMEs, as shown below.

Theoretical modelling revealing the SME physics

Density functional theory calculations were performed to unveil the corresponding atomic configurations of the two switchable states. Details of our calculations can be found in the Methods and Supplementary Information. While tens of Gd adsorption configurations were considered (Supplementary Figs. 6-8 and Supplementary Tables 1 and 2), two of them, denoted configurations Gd-I and Gd-IV, are significantly more stable, by over 400 meV, than the others. The role of Au electrodes was considered by including an Au(111) substrate in further discussion. The reorientation of the molecular dipole by rotating the C₈₂ cage on the Au electrode is checked for the electric switching mechanism. Calculations indicate it unlikely to happen under a reasonably strong electrical field (Supplementary Fig. 9 and Supplementary Table 3). Figure 4a shows the geometric details of configurations Gd-I and Gd-IV where the Gd atom sits over two neighbouring C₆ hexagonal rings as marked with red and blue coloured hexagons, respectively. Configuration Gd-IV is ~6.1 meV more stable than configuration Gd-I, which makes it easy to be switched through an external electric field.

The energy levels for these two states could be extracted using a capacitance model from the data shown in Fig. 2d,e. We have previously calculated two gate efficiency factors α (see above discussion for $C_g:C_s:C_d$), where $e\alpha V_g$ is the change in the electrochemical potential caused by the gate electrode. The energy difference between two adjacent states plus the Coulomb energy was defined as a pair of adjacent degeneracy points 14 using the equation $\alpha e(V_g(N)-V_g(N+1))=\varepsilon^{N+1}-\varepsilon^N+e^2/(C_s+C_d+C_g)$ (where N is the number of electron charge, $\alpha=(C_g+C_s+C_d)/C_g$). The molecular energy levels are extracted from the degeneracy points of Fig. 2e,d and are marked in Fig. 4b,c, respectively.

-8

respectively.

ARTICLES

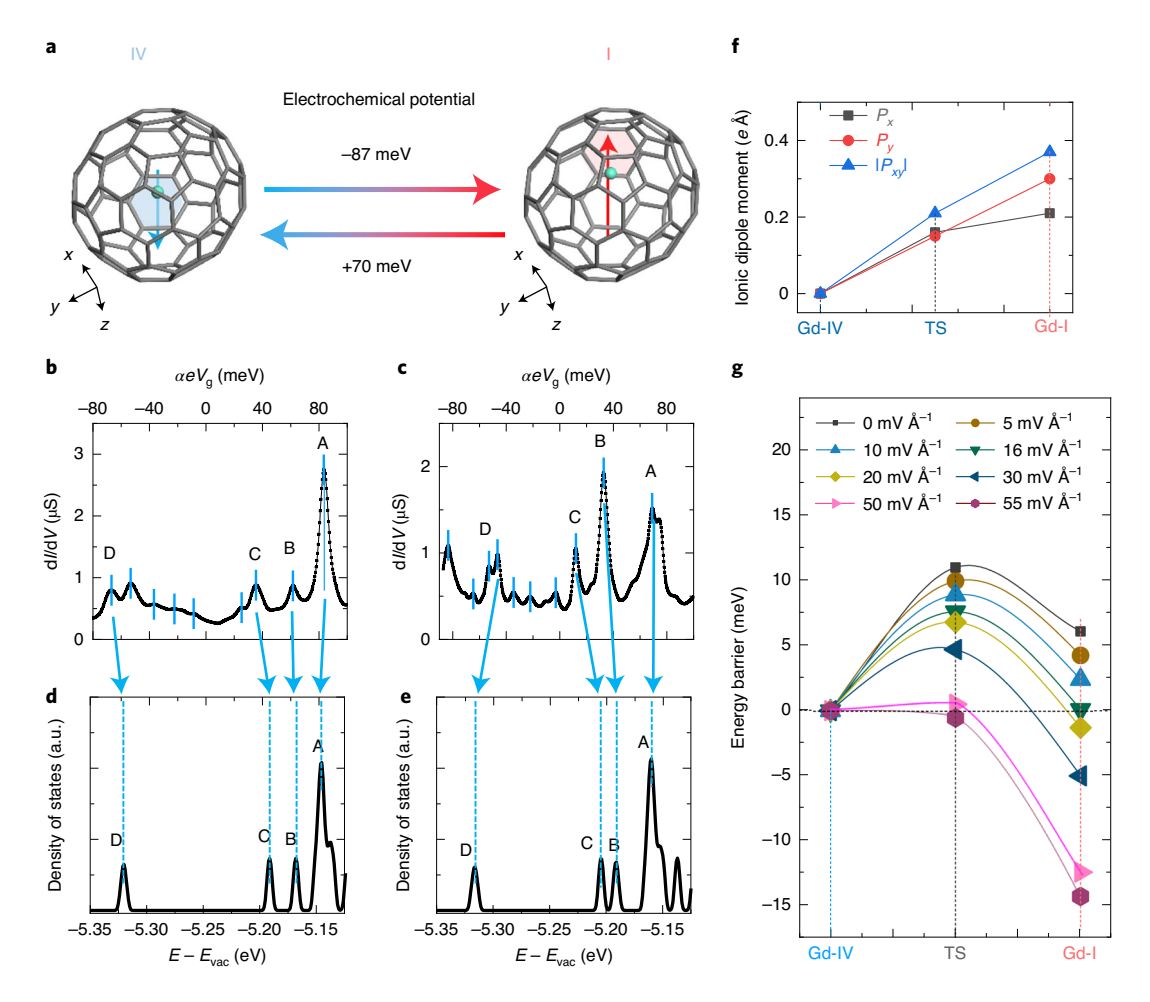


Fig. 4 | Density functional theory calculations revealing the SME physics. a, The switching is interpreted as a transition between Gd-IV and Gd-I. The left and right are the two configurations (Gd-IV, Gd-I), respectively. Two coloured arrows represent the direction of the dipoles. Changing the electrochemical potential of the $Gd@C_{82}$ SMD by >70 meV transforms the molecule from Gd-IV to Gd-I, which will be maintained until a reverse (negative) shift with a magnitude >87 meV occurs. This can be simplified as the gate field driven flipping of the electric dipole of a single $Gd@C_{82}$ molecule, that is, a SME. **b,c**, Differential conductance plotted against the effective molecular orbital gating αeV_g with the bias voltage V_{ds} at 0 V. Extracted from the experimental data of Fig. 2e,d respectively. **d,e**, Theoretical density of states of occupied states near the Fermi levels (-5.09 and -5.10 eV) of the two configurations Gd-IV and Gd-I, respectively. The energy (E) is relative to the vacuum level (E_{vac}). Four characteristic peaks, that is, A to D, are marked in each panel. These agree well with the experimental data in **b** and **c. f**, Ionic dipole moments of the two configurations shown in **a** and the transition state (TS) between them. We used the value of Gd-IV as the zero reference. **g**, Transition pathways and associated energy barriers between configurations Gd-I and Gd-IV under electric fields. The transition barrier might vary in different atomic configurations of contacts.

Figure 4d,e shows the density of states of occupied states near the Fermi levels of configurations Gd-IV and Gd-I, respectively, which qualitatively reproduce the experimentally derived molecular levels. The experimental positions of the four characteristic peaks and the energy differences between them were well reproduced by our present theoretical results, which thus strengthens the assignment of configurations Gd-IV and Gd-I as the two experimental observed states, state 2 and state 1, respectively.

In both the configurations, the Gd atom is prone to adsorb over C_6 rings rather than at the centre of the cage, resulting in stabilized electric dipole moments, that is, a SME. The calculated dipole moments of configurations Gd-IV and Gd-I are illustrated in Fig. 4a, in which red and light blue arrows represent the direction of the dipole moments in the two configurations, respectively. Details of the calculated dipole moments are available in Fig. 4f and Supplementary Table 4. Because a lateral source—drain voltage was applied to the device, we mainly considered the in-plane dipole $|P_{xy}|$ under an electric filed. The switching between the two states can be simplified as an electric-field-driven flipping of the SME of

Gd@ C_{82} . Figure 4g plots the calculated transition pathways from configuration Gd-IV to Gd-I under the electric fields. An electric field of 16 mV Å⁻¹ could switch the relative stability of Gd-I and Gd-IV, with a reduced barrier of 7.6 meV. A field of 50 mV Å⁻¹ could further reduce the barrier to zero. All these values are consistent with our experimentally estimated field of ~33–150 mV Å⁻¹. Given the derived gate efficiencies and the transition voltages, we could infer a potential energy of 87 meV was used by the measured device in transforming from configuration Gd-IV to Gd-I, while the opposite transition needs a potential energy excitation of 70 meV, as illustrated in Fig. 4a. These electronic excitation energies, that is, ~70–87 meV, are high enough to stimulate the Gd atom, surmounting the theoretically predicted thermal transition barrier of 11 meV, which explains the onset of the coercive gate field in Fig. 2b.

Either the applied external electric field or its induced charge doping helps the Gd atom surmount the thermal barrier between configurations Gd-I and Gd-IV. The estimated coercive field of $\sim\!50\,\text{mV}\,\text{Å}^{-1}$ is within range of the experimentally applied field to observe the hysteresis loop that features ferroelectricity (that is, that

features an electret), where the transition occurs when ${\sim}10{-}15\,\mathrm{V}$ voltages act on a ${\sim}10{-}30\text{-nm}$ -thick gate layer. Since the molecule stochastically drops into the gap at a random position, the electrical field cannot always flip the dipole of the molecule once the electric polarization is perpendicular to the gate electrical field. Although we achieve the reproducibility of the reversible switch, it is hard to obtain the same series of Coulomb degeneracy points in different devices, since small differences in contact morphology can lead to different quantized orbits.

Conclusions

The physics of a SME differs from that of ferroelectricity in solids, where the system is stabilized by the exchange coupling between a large number of dipoles in a large domain. Rather, it is more alike to the physics of a single-molecule magnet, where spin polarization is stabilized by the anisotropy energy of individual molecules. Such a SME is free of any inter-dipole coupling, and has been anticipated by recent theories 35 and experimentally tested 19 in long-range ordered crystals, where, however, the inter-dipole coupling is still possible. Our experiment demonstrates the SME at the single-molecule level and thus excludes any inter-dipole coupling, providing convincing evidence of a SME. The position of the single Gd atom inside the $\rm C_{82}$ cage forms the memory storage information unit and may thus lead to miniaturized storage devices in future electronics.

Online content

Any methods, additional references, Nature Research reporting summaries, source data, extended data, supplementary information, acknowledgements, peer review information; details of author contributions and competing interests; and statements of data and code availability are available at https://doi.org/10.1038/s41565-020-00778-z.

Received: 24 December 2019; Accepted: 11 September 2020; Published online: 12 October 2020

References

- Waldrop, M. M. The chips are down for Moore's law. Nature 530, 144–147 (2016).
- Huang, Y. L. et al. Reversible single-molecule switching in an ordered monolayer molecular dipole array. Small 8, 1423–1428 (2012).
- Zhang, J. L. et al. Towards single molecule switches. Chem. Soc. Rev. 44, 2998–3022 (2015).
- Jia, C. et al. Covalently bonded single-molecule junctions with stable and reversible photoswitched conductivity. Science 352, 1443–1445 (2016).
- Blum, A. S. et al. Molecularly inherent voltage-controlled conductance switching. Nat. Mater. 4, 167–172 (2005).
- Wagner, S. et al. Switching of a coupled spin pair in a single-molecule junction. Nat. Nanotechnol. 8, 575–579 (2013).
- Diez-Perez, I. et al. Rectification and stability of a single molecular diode with controlled orientation. Nat. Chem. 1, 635–641 (2009).
- Capozzi, B. et al. Single-molecule diodes with high rectification ratios through environmental control. Nat. Nanotechnol. 10, 522–527 (2015).
- Batra, A. et al. Tuning rectification in single-molecular diodes. Nano Lett. 13, 6233–6237 (2013).
- Sherif, S. et al. Current rectification in a single molecule diode: the role of electrode coupling. Nanotechnology 26, 291001 (2015).
- 11. Park, H. et al. Nanomechanical oscillations in a single- C_{60} transistor. *Nature* 407, 57–60 (2000).

- Lau, C. S. et al. Redox-dependent Franck-Condon blockade and avalanche transport in a graphene-fullerene single-molecule transistor. *Nano Lett.* 16, 170–176 (2016).
- Vincent, R., Klyatskaya, S., Ruben, M., Wernsdorfer, W. & Balestro, F. Electronic read-out of a single nuclear spin using a molecular spin transistor. *Nature* 488, 357–360 (2012).
- Kubatkin, S. et al. Single-electron transistor of a single organic molecule with access to several redox states. *Nature* 425, 698–701 (2003).
- Bai, Z. B. et al. A silicon cluster based single electron transistor with potential room-temperature switching. *Chin. Phys. Lett.* 35, 037301 (2018).
- Gao, L. et al. Graphene-DNAzyme junctions: a platform for direct metal ion detection with ultrahigh sensitivity. Chem. Sci. 6, 2469–2473 (2015).
- Xiao, X., Xu, B. & Tao, N. Changes in the conductance of single peptide molecules upon metal-ion binding. *Angew. Chem. Int. Ed.* 43, 6148–6152 (2004).
- 18. Evangeli, C. et al. Engineering the thermopower of C_{60} molecular junctions. *Nano Lett.* 13, 2141–2145 (2013).
- Kato, C. et al. Giant hysteretic single-molecule electric polarization switching above room temperature. Angew. Chem. Int. Ed. 57, 13429–13432 (2018).
- Pasupathy, A. N. et al. Vibration-assisted electron tunneling in C₁₄₀ transistors. Nano Lett. 5, 203–207 (2005).
- Yu, L. H. & Natelson, D. The Kondo effect in C₆₀ single-molecule transistors. Nano Lett. 4, 79–83 (2004).
- Roch, N., Florens, S., Bouchiat, V., Wernsdorfer, W. & Balestro, F. Quantum phase transition in a single-molecule quantum dot. *Nature* 453, 633–637 (2008).
- Winkelmann, C. B., Roch, N., Wernsdorfer, W., Bouchiat, V. & Balestro, F. Superconductivity in a single-C₆₀ transistor. *Nat. Phys.* 5, 876–879 (2009).
- 24. Danilov, A. V., Kubatkin, S. E., Kafanov, S. G. & Bjornholm, T. Strong electronic coupling between single C₆₀ molecules and gold electrodes prepared by quench condensation at 4 K. A single molecule three terminal device study. *Faraday Discuss.* 131, 337–345 (2006).
- Rosseinsky, M. J. et al. Superconductivity at 28 K in Rb_xC₆₀. Phys. Rev. Lett. 66, 2830–2832 (1991).
- Morton, J. J. L. et al. Environmental effects on electron spin relaxation in N@ C₆₀. Phys. Rev. B 76, 085418 (2007).
- Funasaka, H., Sugiyama, K., Yamamoto, K. & Takahashi, T. Magnetic properties of rare-earth metallofullerenes. *J. Phys. Chem.* 99, 1826–1830 (1995).
- 28. Huang, H., Yang, S. & Zhang, X. Magnetic properties of heavy rare-earth metallofullerenes M@C₈₂ (M = Gd, Tb, Dy, Ho, and Er). *J. Phys. Chem. B* **104**, 1473–1482 (2000).
- de Nadai, C. et al. Local magnetism in rare-earth metals encapsulated in fullerenes. *Phys. Rev. B* 69, 184421 (2004).
- 30. Kitaura, R., Okimoto, H., Shinohara, H., Nakamura, T. & Osawa, H. Magnetism of the endohedral metallofullerenes M@C₈₂ (M = Gd, Dy) and the corresponding nanoscale peapods: synchrotron soft X-ray magnetic circular dichroism and density-functional theory calculations. *Phys. Rev. B* 76, 172409 (2007).
- Okamura, N., Yoshida, K., Sakata, S. & Hirakawa, K. Electron transport in endohedral metallofullerene Ce@C₈₂ single-molecule transistors. *Appl. Phys. Lett.* 106, 043108 (2015).
- Laasonen, K., Andreoni, W. & Parrinello, M. Structural and electronic properties of La@C₈₂. Science 258, 1916–1918 (1992).
- 33. Nuttall, C. J., Hayashi, Y., Yamazaki, K., Mitani, T. & Iwasa, Y. Dipole dynamics in the endohedral metallofullerene La@ C_{82} . Adv. Mater. 14, 293–296 (2002).
- Thijssen, J. M. & van der Zant, H. S. J. Charge transport and single-electron effects in nanoscale systems. *Phys. Status Solidi B* 245, 1455–1470 (2008).
- Quan, X. & Hutchison, G. R. Single molecule ferroelectrics via conformational inversion: an electronic structure investigation. Preprint at https://arxiv.org/abs/1705.09699 (2017).

Publisher's note Springer Nature remains neutral with regard to jurisdictional claims in published maps and institutional affiliations.

© The Author(s), under exclusive licence to Springer Nature Limited 2020

NATURE NANOTECHNOLOGY ARTICLES

Methods

Molecule preparation. Soot containing $Gd@C_{82}$ is produced using the direct current arc discharge method with metal–graphite composite rods in a helium atmosphere. The soot is extracted with carbon disulfide, and the residue is extracted further with pyridine under reflux. $Gd@C_{82}$ molecules are extracted from the cleaned soot using a two-stage high-performance liquid chromatography method. Stage 1 is a preliminary high-performance liquid chromatography process using a Buckyprep column. This yields a fraction containing $Gd@C_{82}$. The second stage involves isolation of $Gd@C_{82}$ from empty fullerenes using a Buckyprep-m column. Sheet samples (1 mm in thickness, 2 mm × 4 mm in area) for measuring the dielectric properties are made by applying pressure to the powdered samples; then the sample is attached with two Au wires and is measured at 2–400 K in a physical property measurement system (Quantum Design PPMS-14 T). The measurements are performed in a frequency range of 40 Hz to 2.00 MHz with Agilent 4294 AV3. The temperature and frequency dependence of the loss tangent results shows evidence for the ferroelectricity behaviour and also the SME.

Device preparation. The ~50-nm-wide gold nanowires are deposited on top of a silicon gate electrode that has previously been oxidized in an oxygen atmosphere to give a SiO₂ layer (~30 nm thick) to act as a gate dielectric. The electrodes and SiO₂ insulator are patterned using an ordinary photolithography procedure, but the nanowire is defined by electron-beam lithography (Fig. 1b inset). When the Au nanowires are prepared, to make sure the chip is clean, the electrodes are cleaned further using oxygen plasma. Then the device containing the $Gd@C_{82}$ is cooled to 1.6 K, and a nanogap is produced using the FCEBJ method¹¹. The current is monitored while the applied voltage between the source and drain is increased. The voltage is decreased to $10\,\mathrm{mV}$ as soon as the current drops by 1%. The cycle is repeated until the resistance is $>1\,\mathrm{M}\Omega$ when the voltage is $20\,\mathrm{mV}$.

Density functional theory calculations. Our density functional theory calculations are performed using the generalized gradient approximation and the projector augmented wave method^{36,37} as implemented in the Vienna ab-initio simulation package³⁸. The kinetic energy cut-off is set to $400 \, \text{eV}$. An $18 \times 18 \times 18 \, \text{Å}^3$ supercell is used to model the isolated Gd@C82 molecule, which ensures a separation of at least 7.5 Å between the molecule and its images. This separation, as previously demonstrated, is sufficient to appreciably reduce the image interactions. The Γ point is used for sampling the first Brillouin zone in all calculations. All atoms are allowed to relax until the residual force on each atom is less than 0.01 eV Å⁻¹. Dispersion interactions are considered at the van der Waals (vdW) density functional level³⁹⁻⁴¹, with the optB86b functional for the exchange potential (optB86b-vdW), which has proven accurate in describing the structural properties of layered materials and is adopted for structure-related calculations^{42–46}. Transition pathways and energy barriers are revealed by the climbing image nudged elastic band method^{47,48}, which locates the exact saddle point of a reaction pathway. Electric dipole moments of the C82 molecule system are calculated on the basis of the classical definition:

$$P = \frac{1}{V} \left(-e \sum_{j} Z_{j} \mathbf{u}_{j} \right) + \int \mathbf{r} \rho(\mathbf{r}) d\mathbf{r}$$
 (1)

Here e is the electron charge, V is the cell volume, Z_j and \mathbf{u}_j are the atomic number and the position of the jth atom and $\rho(\mathbf{r})$ is the electronic charge density at a given location \mathbf{r} in real space. Dipole correction is considered in all calculations to correct the error introduced by the periodic boundary condition and balance the vacuum level differences on the different sides of the polarized molecules 10.4 lelectronic structures are calculated using the Perdew–Burke–Ernzerhof functional 11 with inclusion of spin-orbit coupling on the basis of the optB86b-vdW revealed structures. An on-site Coulomb interaction energy of 6 eV is added to the f orbitals of the Gd atom according to the values reported in the literature f 12.4 f 13.4 f 14.5 f 15.4 f 16.5 f 17.5 f 16.5 f 17.5 f 18.5 f

Analysis of structures. We first consider seven adsorption sites of a single Gd atom adsorption on the inner wall of a C₈₂ molecule (Supplementary Fig. 5 and Supplementary Table 1). In all of these structures, the C₆-Hol site, where a Gd atom sitting over a C₆ hexagonal ring, shows superior stability; its energy is over 1 eV more stable than that of the other two six-carbon-ring sites, and the adsorbed configurations of the other sites transform into the C₆-Hol site (Supplementary Table 1). There are six inequivalent C_6 rings of a C_{82} molecule (Supplementary Fig. 7); we next double-check the relative stability of these six configurations. The relative total energy and the height of the adsorbed Gd atom at every site are listed in Supplementary Table 2. We denote the C₆-Hol configuration we previously obtained as configuration Gd-I, while others are represented as configurations II to VI (Supplementary Fig. 7). Configurations Gd-I and Gd-IV are significantly more stable, while other configurations are at least 400 meV less favoured. We notice that there are three inequivalent C_5 rings and also check the stability of being adsorbed on these previously unconsidered C5 rings. These rings do not offer a more stable configuration (Supplementary Fig. 8).

A Au(111)- 7×7 parallelogram supercell was adopted to model the adsorption of Gd@C₈₂ on the Au(111) surface, which ensures a separation of at least 12 Å among image molecules. We considered nine contact configurations, including

six inequivalent C₆ rings and three inequivalent C₅ rings (denoted as C₈₂-C₆-I to -VI and C₈₂-C₅-a to -c, respectively), of the C₈₂ cage on the Au substrate, as shown with colour-filled hexagons and pentagons in Supplementary Fig. 9. The Gd atom inside the C₈₂ cage was placed at the two previously identified most-stable sites, that is, Gd-IV and Gd-I. Two contact distances representing physisorption and chemisorption were also considered. We ruled out some apparently less stable configurations according to our physisorption and preliminary chemisorption results and listed the relative chemisorption energies of the rest in Supplementary Table 3. It shows that adsorption configuration C_{82} - C_{6} -II is at least 120 meV more stable than the other configurations. The transition barriers among them are even larger than this value, indicating that the reorientation of the molecular dipole by rotating the C₈₂ cage is unlikely under a reasonably strong electrical field. Given the superior stability of these two Gd sites relative to the others (that is, hundreds of meV), we concluded that Gd-I@C82-C6-II and Gd-IV@C82-C6-II (shown in Supplementary Fig. 9 and simplified as configuration Gd-I and Gd-IV in the manuscript) are the two most stable configurations among all our considered configurations.

Data availability

The data shown in the paper are available at https://doi.org/10.6084/m9.figshare.12720392. Source data are provided with this paper.

Code availability

The density functional theory program used to analyse the results is available from the corresponding author on reasonable request.

References

- Blöchl, P. E. Projector augmented-wave method. *Phys. Rev. B* 50, 17953–17979 (1994).
- Kresse, G. & Joubert, D. From ultrasoft pseudopotentials to the projector augmented-wave method. *Phys. Rev. B* 59, 1758–1775 (1999).
- Kresse, G. & Furthmüller, J. Efficient iterative schemes for ab initio total-energy calculations using a plane-wave basis set. *Phys. Rev. B* 54, 11169–11186 (1996).
- Lee, K., Murray, É. D., Kong, L., Lundqvist, B. I. & Langreth, D. C. Higheraccuracy van der Waals density functional. *Phys. Rev. B* 82, 081101 (2010).
- Dion, M., Rydberg, H., Schroder, E., Langreth, D. C. & Lundqvist, B. I. Van der Waals density functional for general geometries. *Phys. Rev. Lett.* 92, 246401 (2004).
- 41. Klimeš, J., Bowler, D. R. & Michaelides, A. Van der Waals density functionals applied to solids. *Phys. Rev. B* 83, 195131 (2011).
- Hong, J. et al. Exploring atomic defects in molybdenum disulphide monolayers. *Nat. Commun.* 6, 6293 (2015).
- Qiao, J., Kong, X., Hu, Z. X., Yang, F. & Ji, W. High-mobility transport anisotropy and linear dichroism in few-layer black phosphorus. *Nat. Commun.* 5, 4475 (2014).
- Qiao, J. et al. Few-layer tellurium: one-dimensional-like layered elementary semiconductor with striking physical properties. Sci. Bull. 63, 159–168 (2018).
- Zhao, Y. et al. Extraordinarily strong interlayer interaction in 2D layered PtS₂. Adv. Mater. 28, 2399–2407 (2016).
- Zhao, Y. et al. High-electron-mobility and air-stable 2D layered PtSe₂ FETs. Adv. Mater. 29, 1604230 (2017).
- Sheppard, D., Terrell, R. & Henkelman, G. Optimization methods for finding minimum energy paths. J. Chem. Phys. 128, 134106 (2008).
- Sheppard, D., Xiao, P., Chemelewski, W., Johnson, D. D. & Henkelman, G. A generalized solid-state nudged elastic band method. *J. Chem. Phys.* 136, 074103 (2012).
- Neugebauer, J. & Scheffler, M. Adsorbate-substrate and adsorbateadsorbate interactions of Na and K adlayers on Al(111). Phys. Rev. B 46, 16067–16080 (1992).
- Ding, W. et al. Prediction of intrinsic two-dimensional ferroelectrics in In₂Se₃ and other III₃-VI₃ van der Waals materials. Nat. Commun. 8, 14956 (2017).
- Perdew, J. P., Burke, K. & Ernzerhof, M. Generalized gradient approximation made simple. *Phys. Rev. Lett.* 77, 3865–3868 (1996).
- Petersen, M., Hafner, J. & Marsman, M. Structural, electronic and magnetic properties of Gd investigated by DFT+U methods: bulk, clean and H-covered (0001) surfaces. J. Phys. Condens. Matter 18, 7021–7043 (2006).
- 53. Tao, K. et al. Self-consistent determination of Hubbard U for explaining the anomalous magnetism of the Gd₁₃ cluster. Phys. Rev. B 89, 085103 (2014).
- Harmon, B. N., Antropov, V. P., Liechtenstein, A. I., Solovyev, I. V. & Anisimov, V. I. Calculation of magneto-optical properties for 4f systems: LSDA + Hubbard U results. J. Phys. Chem. Solids 56, 1521–1524 (1995).

Acknowledgements

We gratefully acknowledge the financial support of the National Key R&D Program of China (2017YFA0303203, 2018YFE0202700, 2018YFA0306004 and 2016YFA0300101), the National Natural Science Foundation of China (U1732273, 21973038, 91961101, 61761166009, 11522432, 11574217, U1732159, 61822403, 11874203, 11904166,

11622437, 61674171, 11974422, 21721001, 91961112, 11227904, 61521001 and 61801209), the Strategic Priority Research Program of Chinese Academy of Sciences (grant no. XDB30000000), the Fundamental Research Funds for the Central Universities, China, and the Research Funds of Renmin University of China (grants no. 16XNLQ01 and 19XNQ025), the Fundamental Research Funds for the Central Universities (020414380082, 020414380127, 020414380150 and 020414380151) and the opening Project of the Wuhan National High Magnetic Field Center. C.W. was supported by the Outstanding Innovative Talents Cultivation Funded Programs 2017 of Renmin University of China. Calculations were performed at the Physics Lab of High-Performance Computing of Renmin University of China and Shanghai Supercomputer Center. S.-E.S. acknowledges support from NSF Career Grant DMR-1945420 and NYSTAR through Focus Center-NY-RPI contract C150117. We thank H.-L. Cai from Nanjing University for stimulating discussions. We also thank S.-T. Zhang from Nanjing University for preparing bulk materials.

Author contributions

F.S. conceived the research and B.W., W.J., S.-Y.X., S.-F.S. and M.A.R. co-supervised the project. M.Z. performed the bulk material measurements. C.W. and W.J. performed and analysed the density functional theory calculations. Z.B. designed and fabricated the devices. K.Z. performed the SMD measurements. F.-F.X. performed high-performance

liquid chromatography for purification of the molecular materials. Y.-Z.T. participated in the separation of the molecular materials. S.-Y.X. prepared the molecular materials. X.T. and D.P. assisted in the device fabrication. Y.G. and J.W. assisted with the density functional theory calculations. K.Z., C.W., E.S., W.J. and M.A.R. wrote the paper. K.-J.H., L.C., S.Z., L.K., J.C., P.W., X.W., J.L., Y.S. and G.W. participated in discussions on this manuscript. All authors discussed the results and commented on the manuscript.

Competing interests

The authors declare no competing interests.

Additional information

Supplementary information is available for this paper at https://doi.org/10.1038/s41565-020-00778-z.

Correspondence and requests for materials should be addressed to F.S., W.J., S.-Y.X., S.-F.S. or M.A.R.

Peer review information *Nature Nanotechnology* thanks Sadafumi Nishihara and the other, anonymous, reviewer(s) for their contribution to the peer review of this work.

Reprints and permissions information is available at www.nature.com/reprints.